A Supramolecular–Quantum Dot System for Broad-Spectrum Detection of Fentanyl Analogues

Yanjing Gao,[1,#] Farbod Shirinchi,[1,#] Audrey Hansrisuk,[1] Runyao Zhu,[1] Sijie Xian,[1] Marya Lieberman,[2] Matthew J. Webber[1,*] and Yichun Wang[1,*]

[1] Department of Chemical & Biomolecular Engineering
[2] Department of Chemistry & Biochemistry
[#] YG and FS contributed equally to this work
[*] University of Notre Dame
Notre Dame, IN 46556, USA
E-mail: mwebber@nd.edu or ywang65@nd.edu

Abstract: Synthetic opioids, especially fentanyl and its analogues, have led to an epidemic of abuse and a significant increase in overdose deaths in the United States. Current detection methods have significant drawbacks in their sensitivity, scalability, and portability that limit use in field-based applications to promote public health and safety. The need to detect trace amounts of fentanyl in complex mixtures with other drugs or interferents, and the continued emergence of new fentanyl analogues, further complicates detection efforts. Accordingly, there is an urgent need to develop convenient, rapid, and reliable sensors for fentanyl detection. In this study, a sensor is prepared based on competitive displacement of a fluorescent dye from the cavity of a supramolecular macrocycle, with subsequent fluorescence quenching from graphene quantum dots. This approach can detect and quantify small quantities of fentanyl along with 58 fentanyl analogues, including highly potent variants like carfentanil that are of increasing concern. Furthermore, selective detection of these agents is possible even when at 0.01 mol% in the presence of common interferents. Results are provided within seconds, with stable performance over time. This simple, rapid, reliable, sensitive, and cost-effective approach couples supramolecular capture with graphene quantum dot nanomaterial quenchers to create a tool with the potential to advance public health and safety in the context of field-based detection of drugs in the fentanyl class.

Introduction

The opioid epidemic, and in particular the abuse of fentanyl and its analogues, is a major public health crisis and also poses a serious security threat.(1) Fentanyl is a potent synthetic opioid with anesthetic and analgesic function derived from binding and subsequent activation of the μ-opioid receptor,(2, 3) with potency far-surpassing that of heroin (30-50 fold) and morphine (50-100 fold).(4) In addition, its high lipophilicity leads to enhanced brain distribution relative to these other agents.(5) The enhanced potency and more rapid action of fentanyl is beneficial in the treatment of severe pain, such as that associated with cancer or surgery.(6) However, these characteristics also lead to a high rate of physical dependence and addiction, with attendant risks for abuse and lethal overdose.(4) The accessible synthesis of fentanyl and its analogues has also made these agents pervasive as drugs of abuse, with fentanyl commonly included in street drugs such as heroin or cocaine to boost their potency.(6, 7) Drug users may unknowingly consume substantial quantities of fentanyl; with an estimated LD_{50} of only ~30 μg/kg,(8, 9) its potency and wide-spread availability contributes to an alarming surge in fentanyl-related overdose deaths in the United States since 2013.(10)

New technologies are needed to combat this growing fentanyl crisis, specifically in the detection of trace concentrations of fentanyl in complex mixtures with other drugs or inactive excipients.(11-13) Currently available methods rely on liquid/gas chromatography-mass spectrometry (LC/GC-MS),(14, 15) quantitative nuclear magnetic resonance spectroscopy (qNMR),(16) and surface-enhanced Raman spectroscopy (SERS)(17-19) to identify and quantify fentanyl with high sensitivity and specificity, especially from complex mixtures. However, these techniques require expensive instrumentation operated by technically-trained experts in a laboratory setting; tedious pretreatment procedures and complicated surface modification techniques also present barriers to widespread implementation.(16) Alternatively, colorimetric tests,(20) immunoassays,(21, 22) portable Raman spectrometers,(23) and handheld SERS devices(24) offer relative ease in operation, rapid response, and cost-effectiveness. However, many of these can be poorly quantitative, have low sensitivity, and struggle with detection of fentanyl in mixture due to both false-positive and false-negative results.(24-28) Lateral flow immunoassays offer a point-of-use approach to detect the presence of fentanyl, and though these rely on specific antibodies, their lack of molecular specificity yields false-positive results in the presence of moderate concentrations of interferents;(21, 22) these also struggle to detect certain fentanyl analogues with modifications to the 4-piperidinyl (*e.g.,* carfentanil) or carbonyl moieties.(21, 29, 30) DNA aptamer-based sensors can specifically detect and quantify fentanyl and some of its analogues, with no response to other illicit drugs, cutting agents, or adulterants.(31, 32) However, these sensors have limitations in detecting modified fentanyl analogues, and may require costly and time-consuming discovery of new aptamers in response to emergent variants. In addition, the long-term stability of aptamer-based electrochemical sensors may limit certain practical applications.(33) Accordingly, there remain ongoing challenges in achieving convenient, efficient, low-cost, stable, highly sensitive, and specific detection of fentanyl and its analogues in complex mixtures.

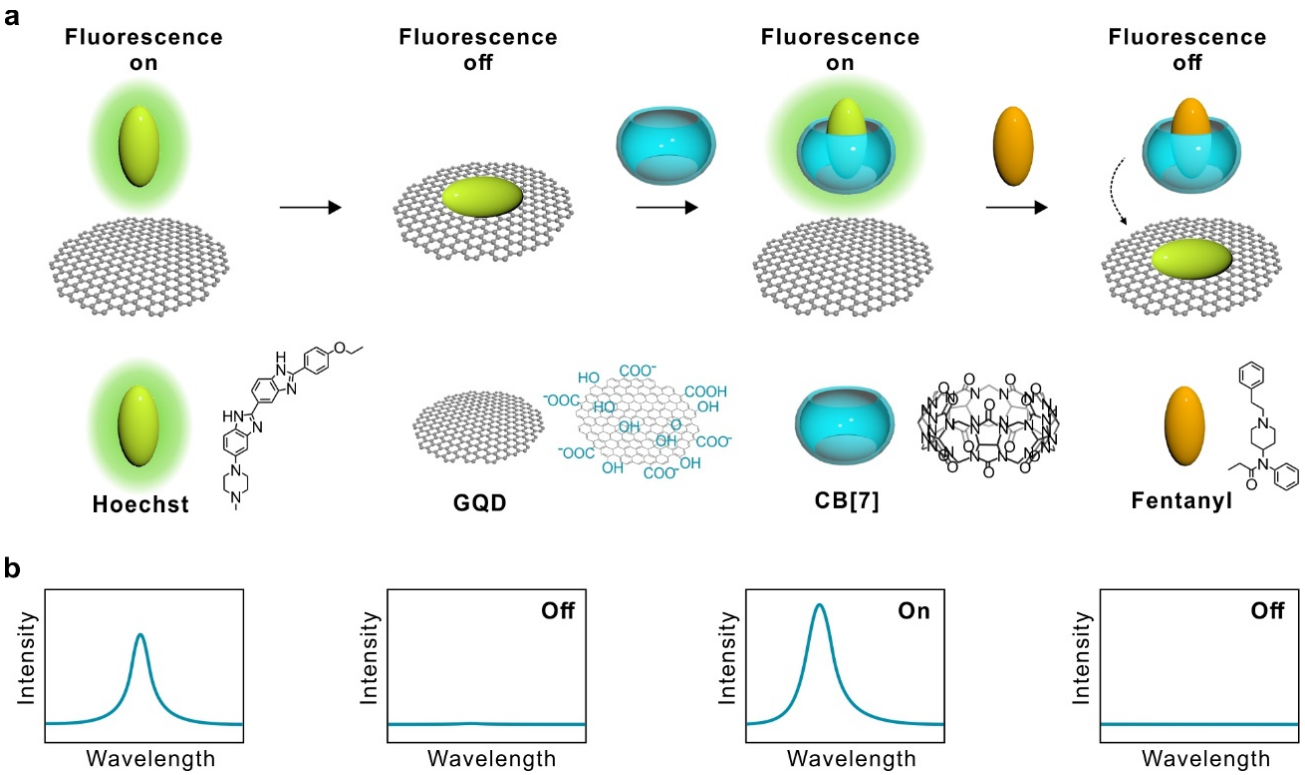

Scheme 1. Fentanyl detection based on an HO/GQD/CB[7] fluorescence sensor. (a) Scheme of the step-by-step assembly of the HO/GQD/CB[7] fluorescence sensor for fentanyl detection. (b) Illustrative demonstration of the expected HO fluorescence intensity following each step of the step-by-step sensor assembly and use for fentanyl detection.

Supramolecular macrocycles offer opportunities for affinity-mediated capture and detection of certain small molecule analytes,(34) including fentanyl and related drugs of abuse.(35) One macrocycle in particular, cucurbit[7]uril (CB[7]), is a water-soluble host cavitand composed of seven repeating glycoluril units that offers high-affinity binding to a diverse array of small molecule guests.(36-38) The binding affinity of CB[7] has been investigated in applications spanning drug delivery, sensing, imaging, nerve block reversal, protein isolation, and label-free enzyme assays.(39-43) Fentanyl is known to bind CB[7] with an affinity (K_{eq}) of 1.8 x 10^7 M^{-1},(35) offering a potentially useful capture agent for integration with detection platforms.(44, 45) In particular, studies using ^{1}H NMR showed that CB[7] binds to a characteristic phenethylamine motif present in many fentanyl analogues.(45) Covalently tethering CB[7] to the surface of silver nanoparticles for use in SERS detection enabled clear detection down to at least 0.5 nM.(45) However, non-specific adsorption of the highly surface-active fentanyl to the colloid surface prevented CB[7]-based selective capture for SERS detection, and thus CB[7] recognition did not offer meaningful signal enhancement for use in SERS sensing. Another approach prepared a fluorescence sensor based on reversible aggregation of gold nanoclusters (AuNCs) using CB[7], where fentanyl binding reduced the extent of AuNC aggregation.(44) This sensor achieved a detection limit of ~3 nM with favorable selectivity in the presence of other illicit drugs, though relied on a complex design requiring peptide-modified AuNCs to achieve this function. Recently, a colorimetric assay was demonstrated by fentanyl-mediated competitive release of a ferrocene catalyst from CB[7], prompting substrate conversion in solution.(46) This assay could detect fentanyl and two tested fentanyl analogues at concentrations of approximately 5 mM or above, though no efforts were taken to quantify fentanyl in mixture with other interferents. Quantification using this mechanism based on a catalytic read-out is inherently sensitive to variables like incubation time and operating temperature, while the limit of detection may not be suitable for certain applications necessitating detection of trace quantities of fentanyl.

A CB[7]-based fluorescent sensor is demonstrated here that offers a simple design, rapid and field-ready readout, and quantitative performance. This fentanyl sensor (***Scheme 1***) is prepared by multi-step assembly of a Hoechst 33342 (HO) fluorescent reporter, a quencher (graphene quantum dots, GQDs), and a fluorescence enhancer (CB[7]). HO is a cationic and weakly fluorescent dye in aqueous solution, yet exhibits enhanced fluorescence upon its binding to CB[7].(47) The free cationic HO dye readily adsorbs to negatively charged GQD, leading to a “turn off” in its fluorescence *via* energy transfer and quenching with the polyaromatic GQD. The addition of CB[7] to the HO/GQD complex desorbs HO by CB[7]–HO complexation, resulting in fluorescence “turn on” that is enhanced beyond the fluorescence of HO alone in solution. When a guest with higher affinity for CB[7] binding, such as fentanyl (K_{eq} = 1.8 x 10^7 M^{-1})(35) is introduced to the HO/GQD/CB[7] mixture, fentanyl displaces HO, which again adsorbs to the GQD to be quenched, leading to a fluorescence “turn off” response. The change in fluorescence from “on” to “off” for this sensor system provides quantitative detection of fentanyl down to nanomolar concentrations, including when in

the presence of common interferents. This detection method also can detect emerging potent fentanyl analogues, including carfentanil, that are becoming increasingly available. Accordingly, based on its selectivity in the presence of common interferents and ability to recognize at least 58 fentanyl analogues, the present approach improves on the drawbacks of many detection methods, especially conventional immunoassays. In addition, this sensor provides rapid response within seconds, with long-term stability in performance. As such, pairing of supramolecular capture and quenching from graphene quantum dots leads to a sensor with promise for routine, quantitative, and field-ready detection of fentanyl and its analogues.

Results & Discussion

Sensor Synthesis and Characterization. The envisioned sensor entailed competition-mediated displacement of a fluorescent dye from the portal of CB[7] by fentanyl, to then be quenched once free in solution by GQDs, leading to a read-out comprising a fluorescence turn-off response (***Scheme 1***). CB[7] was synthesized according to established methodology to serve as the supramolecular capture agent.(48) Pristine GQDs were synthesized as the fluorescence quencher using modification of previously reported methods,(49, 50) and revealed by high resolution transmission electron microscopy (TEM) to have a size of 7.3 ± 1.2 nm (***Figure 1a***) with a zeta potential of -21.0 ± 2.4 mV. Additional characterization of pristine GQDs can be found in ***Section S.3*** of the *Online Supporting Information*.

Selection of a fluorescent reporter dye entailed specific considerations for function of the envisioned sensor. Namely, the binding affinity of this reporter should be lower than the target analyte of interest, fentanyl (1.8 x 10^7 M^{-1})(35) in this case, to enable competition-mediated dye displacement for sensor read-out. Moreover, the dye must efficiently bind to the GQD quencher; the negative surface charge of GQD offers a binding preference for positively charged dyes. An initial screen was performed on multiple different cationic dyes that were expected to bind to both CB[7] and GQDs, including Hoechst 33342 (HO), acridine orange (AO), and Rhodamine B (RhB), to determine their utility to function in this role (***Figure S3***). HO fluorescence was completely quenched upon addition of GQDs, yet was readily rescued and even enhanced upon addition of CB[7] (***Figure S3a***) In contrast, AO (***Figure S3b***) and RhB (***Figure S3c***) did not offer similar function, as RhB was not effectively "turned off" by GQD, while AO was not desorbed and "turned on" by CB[7]. Though RhB has been reported to bind and be quenched by GQDs through a combination of π-π and electrostatic interactions,(51) quenching was not observed in the concentration regime explored here. AO, meanwhile, is a known guest for CB[7] with a moderate affinity of 2 × 10^5 M^{-1},(52) yet this interaction was not sufficient to desorb it from the GQDs. In this preliminary screen, HO was thus shown to offer a good balance of adsorption of GQDs with desorption and fluorescence enhancement upon addition of CB[7].

HO was therefore further explored as a cationic fluorescent guest of CB[7]. The fluorescence emission (λ_{ex} = 350 nm) of HO has a peak at ~500 nm (***Figure 1b***). Addition of pristine

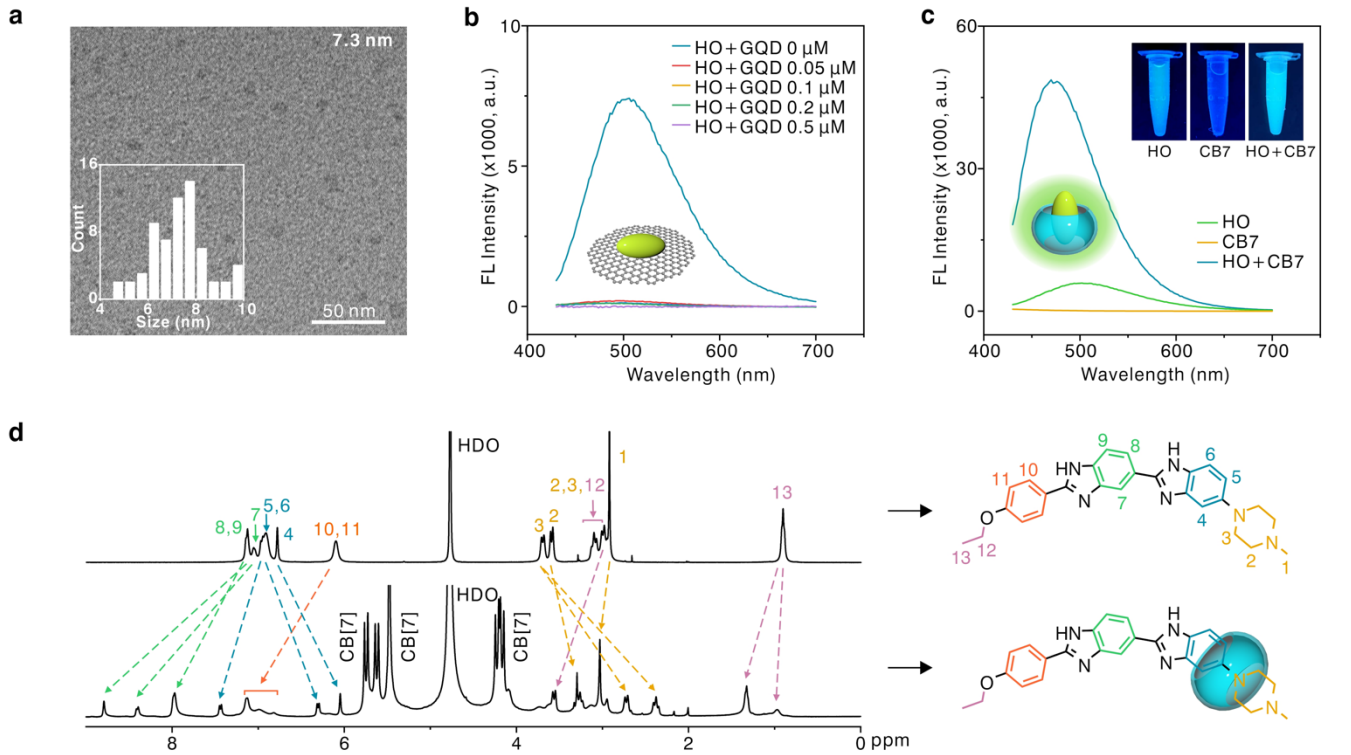

Figure 1. Characterization of sensor components of GQDs, HO, and CB[7]. (**a**) Transmission electron microscopy (TEM) image and size distribution (*inset*) of pristine GQDs. (**b**) Fluorescence spectra of HO (0.25 μM) with GQD added at various concentrations (λ_{ex} = 350 nm). (**c**) Fluorescence spectra of HO, CB[7], and the CB[7]–HO complex (λ_{ex} = 350 nm). (**d**) ^{1}H NMR spectra of HO (*top*), and a 1:1 mixture of HO with CB[7] (*bottom*). Protons are labeled according to the structure shown, revealing the likely interaction mode of HO with CB[7].

GQDs resulted in a concentration-dependent "turn off" of HO fluorescence. In spite of comparable excitation/emission profiles for HO and GQD, the fluorescence of the latter was negligible by comparison and could be readily subtracted as a background in all experiments. Combining HO with CB[7] in the absence of GQDs led to a significant (~10x) enhancement in peak emission intensity (***Figure 1c***), as well as a pronounced blue shift from ~500 nm to ~470 nm. This enhanced fluorescence arises from the inclusion effect, as the fast torsional motion of the fluorophore is restricted upon inclusion and is also protected from water; these effects inhibit nonradiative relaxation and lead to fluorescence enhancement of the complexed dye.(*47*, *53-55*) The ^{1}H NMR spectra of HO demonstrated evidence of binding CB[7], with shifting in specific protons pointing to a likely mode of inclusion complex formation involving portal alignment with the cationic tertiary amino groups on the HO (***Figure 1d***). A preference to bind HO by inclusion of nonpolar groups within the cavity and simultaneous electrostatic interactions between cationic charges on the guest and the electronegative carbonyls of the CB[7] portal aligns with expectations for CB[7]–guest binding. Though the CB[7]–HO interaction was previously measured in buffer,(*47*) which can introduce competition from cations,(*56*) its affinity was determined here using both isothermal titration calorimetry (2.3 x 10^{6} M^{-1}, ***Figure S4a***) and fluorescence (3.9 x 10^{6} M^{-1}, ***Figure S4b***) in DI water, according to operational sensor conditions.

Sensor Validation with Model Guests. To establish proof-of-principle for the HO/GQD/CB[7] sensor to detect fentanyl in DI water, a series of model guests were first investigated, including hexamethylenediamine (HE), 3,3'-(octane-1,8-diyl)-bis-(1-ethyl-imidazolium) (BI), *p*-xylylenediamine (PX), and 1-adamantanol (AD). These model guests have known binding affinities to CB[7] of ~10^{7} M^{-1} (HE and BI), ~10^{9} M^{-1} (PX), and ~10^{10} M^{-1} (AD).(*57*, *58*) The sensor was initially constructed through step-by-step assembly of HO, pristine GQDs, and CB[7], with a fixed molar concentration ratio of HO:GQD:CB[7] of 1:2:1. The successful construction was confirmed by distinct fluorescence transitions between "off" and "on" states upon addition of CB[7] (***Figure 2a***, ***Figures S5-6***). Model guests were then introduced into the sensor system at a fixed molar concentration ratio of HO:GQD:CB[7]:model guest of 1:2:1:1. The introduction of model guests triggered competitive displacement of the HO dye from the CB[7] cavity, enabling rebinding of HO to pristine GQDs and yielding a near-complete "turn off" of sensor fluorescence (***Figure 2a***, ***Figures S5-6***). Utilizing the CB[7]–HO complex as a sensor without quenching from pristine GQDs resulted in no quenching of HO fluorescence upon its competition-mediated displacement into solution, and resulted in a discernible background signal (***Figure S7***). The HO/GQD/CB[7] fluorescent sensor was therefore an excellent candidate for model guest detection due to its enhanced signal-to-noise that resulted from coupling the fluorescent enhancement of the CB[7]–HO complex alongside the quenching by adsorption of displaced HO to GQDs.

Fluorescence switch-off efficiency, $(F_0\text{-}F)/F_0$, was next defined as a metric to quantify sensitivity, where F_0 and F represent the fluorescence of the sensor before and after addition of model guest, respectively. Upon addition of known quantities of model guests, the sensor fluorescence decreased with increasing model guest concentration (***Figure 2b***). The resultant switch-off efficiency curves displayed a linear relationship within the concentration range of 1-100 nM for the model guests (***Figure 2c***). The calculated limits of detection (LOD) derived from these linear relationships were 7.6 nM (HE), 9 nM (BI), 6.1 nM (PX), and 3.0 nM (AD), suggesting highly sensitive detection across a spectrum of model guests. The switch-off efficiency curves of model guests were established for CB[7]–HO in the absence of pristine GQDs, resulting in lower switch-off efficiency and higher limits of detection compared to that achieved by the HO/GQD/CB[7] sensor across various concentrations of model guest (***Figure S8***). This observation demonstrates the importance of including pristine GQDs in the HO/GQD/CB[7] sensor for improved sensitivity compared to what could be achieved simply from competition-mediated displacement of HO from CB[7] without the addition of solution-phase quenching.

The sensor displayed a rapid response, as evidenced by recording fluorescence decay curves upon the addition of varying concentrations of model guest (***Figure 2d***). The fluorescence change after 2 µL of DI water was added to 200 µL of the sensor solution was negligible, meaning sample dilution alone did not significantly shift the binding equilibrium for CB[7]–HO recognition. However, upon addition of a model guest (HE) at concentrations of 0.25-5 µM, the fluorescence after 2 µL was added to 200 µL of the sensor solution rapidly decreased due to the displacement of HO by HE and fluorescence quenching of free HO by GQD. Fluorescence decay rates generally increased with higher concentrations of model guest, reaching zero within a few minutes in all cases. The addition of a manual mixing step, lasting ~8 s, resulted in effectively instant fluorescence reduction upon initiating data collection (***Figure S9a***). The duration of function for the sensor was studied by measuring stability of its baseline "on" state over time. Despite some decrease in fluorescence of the sensor solution with continuous monitoring for 20 d (***Figure 2e***), the sensor retained high signal and rapid response capabilities (***Figure S9b***), supporting long-term stability. Comparatively, methods based on LC/GC-MS,(*11*, *14*, *15*) qNMR,(*16*) SERS,(*59*) and immunoassays have time-intensive sample preparation, prolonged incubation times, and/or issues with long term stability.

In its role as a reporter, HO performs exceptionally well; it is quenched with very limited fluorescence in the presence of GQDs, but its fluorescence is readily rescued by introduction of CB[7], enabling its use to detect model guests with affinities in excess of its own binding to CB[7]. Comparatively, other cationic dyes like AO and RhB did not have similar function (***Figure S3***) in spite of known interactions with CB[7] and/or GQDs; AO was not effectively desorbed from GQDs by addition of CB[7], while RhB was not effectively bound and quenched by GQDs. It is therefore gathered from these results that the effective affinities of HO for CB[7] inclusion (measured

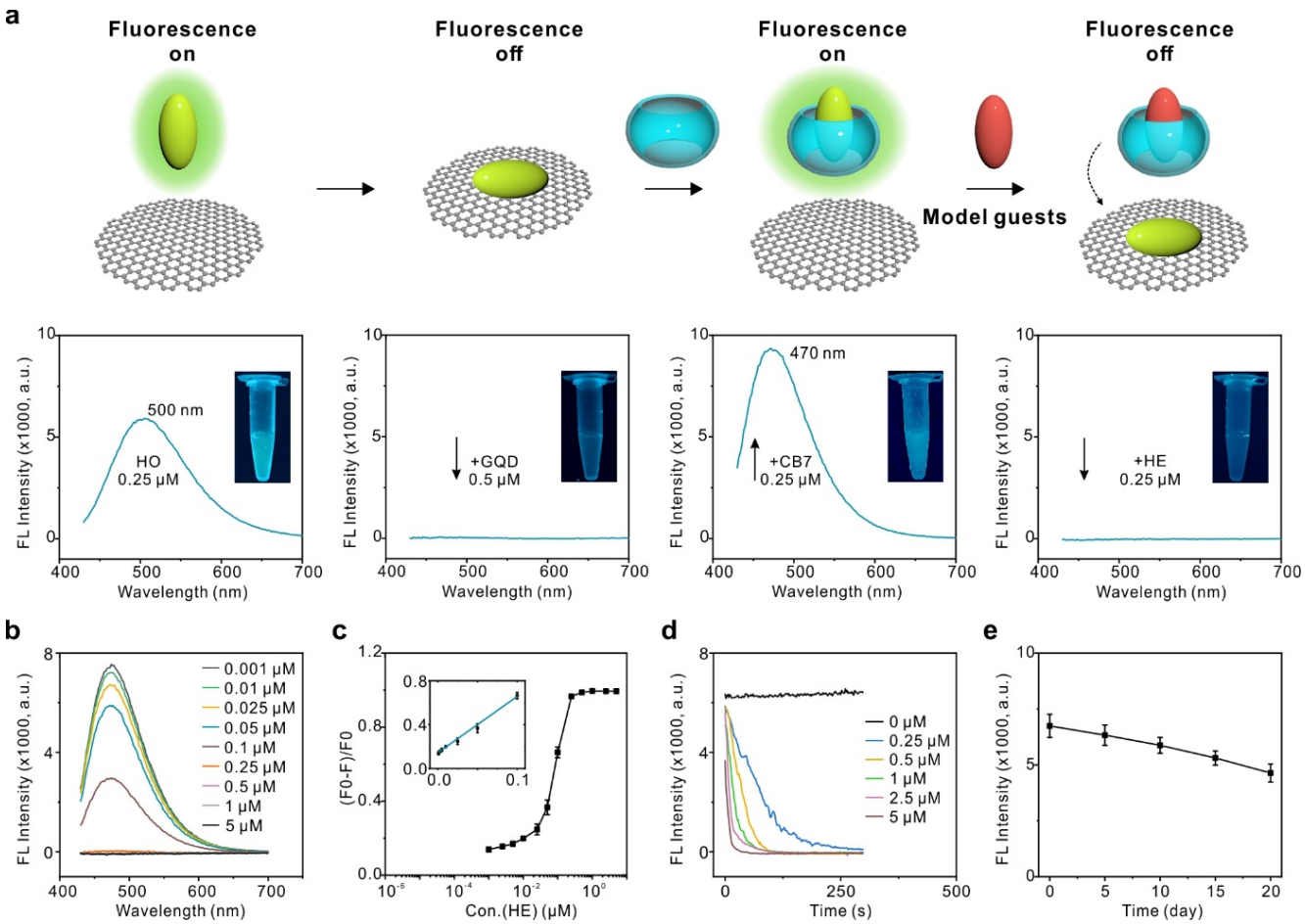

Figure 2. Performance of the HO/GQD/CB[7] sensor in detection of model guests. (a) Fluorescence toggling: "off" – "on" – "off" upon sequential addition of pristine GQDs, CB[7], and model guest (HE) into HO solution. (**b**) Fluorescence spectra of the sensor upon increasing the concentration of HE as a model guest. (**c**) Switch-off efficiency curve and linear response (*inset*) for assays using the sensor with varied concentrations of HE as a model guest. A connecting line is shown for the full concentration range only to aid in visualization of the trend. (**d**) Fluorescence response of the sensor upon the addition of HE as a model guest (λ_{ex}= 350 nm, λ_{em}= 470 nm). (**e**) Baseline fluorescence for the HO/GQD/CB[7] sensor over time.

here as ~10^6 M^{-1}) and GQD adsorption are nearly identical, allowing a portion of the fluorescent signal to be rescued upon introduction of CB[7], with HO in equilibrium between CB[7]- and GQD-bound states when all three species are present at similar concentration. Indeed, further investigation of raw fluorescence intensities supports this hypothesis of affinity-matched binding. The fluorescence of free HO at 0.25 μM was fully quenched upon addition of only 0.05 μM GQDs (***Figure S10a***). The addition of CB[7] at 0.25 μM led to the expected HO fluorescence enhancement, yet as GQDs were added over a range of 0.05-0.5 μM, a concentration-dependent quenching effect was observed (***Figure S10b***). However, even with GQDs present at an apparent excess, some HO fluorescence was maintained when CB[7] was present. Accordingly, HO was found to be an optimal fluorescence reporter for use in subsequent experiments. In the specific context of fentanyl detection, the CB[7]–HO interaction (~10^6 M^{-1}) is lower than that reported for CB[7]–fentanyl (~10^7 M^{-1}).(*35*) The HE model guest has comparable affinity for CB[7] as that of fentanyl and HE enabled efficient sensor turn-off, lending further support for the possibility that the HO/GQD/CB[7] sensor could be used for florescent detection of fentanyl by a similar competitive displacement and quenching mechanism.

Sensor Performance with GQD Size and Charge. The size of GQDs have been reported as an important factor governing their interaction with fluorescent dyes,(*60*, *61*) and this may have implications for the switch-off efficiency of the system here. Thus, GQD was explored with two additional sizes, 18.2 ± 2.7 nm and 36.2 ± 8.6 nm (***Figure 3a,b***). The corresponding zeta potential of the larger GQDs, named GQDs (18.2) and GQDs (36.2), were -15.1 ± 3.8 mV and -9.4 ± 2.8 mV, respectively (***Figure 3c***). The decrease in negative charge for larger GQDs compared to the 7.3 nm GQDs used in the initial screen (-21.0 ± 2.4 mV) is expected; larger GQDs contain a higher number of edge carboxylic groups proportional to their lateral size, yet the surface area of GQDs grows quadratically with their lateral size, thereby reducing the density of carboxylic groups.(*61*) GQDs with varying sizes were explored for their sensing performance as fluorescence quenchers. In comparison with smaller pristine GQDs, it was observed that

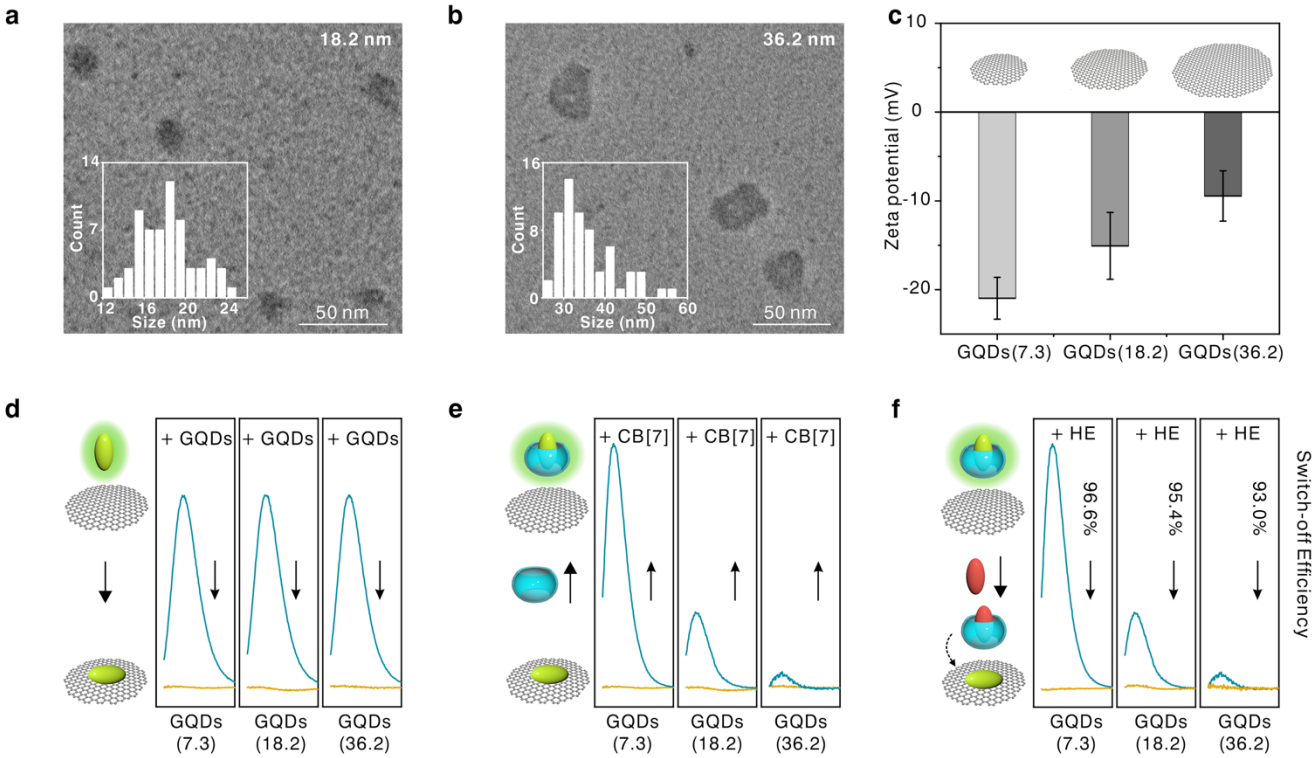

Figure 3. Impact of GQDs size on HO/GQD/CB[7] sensor performance. (**a-b**) TEM images and size distributions of GQDs in two distinct and larger size ranges of 18.2 nm (**a**) and 36.2 nm (**b**). (**c**) Zeta potentials of small pristine GQDs (7.3), medium GQDs (18.2), and large GQDs (36.2). (**d-f**) Fluorescence toggling: "off" – "on" – "off" upon addition of (**d**) 0.5 μM pristine GQD (7.3), GQD (18.2) or GQD (36.2) (*yellow*), (**e**) 0.25 μM CB[7] (*blue*), and (**f**) 0.25 μM HE (*yellow*) into HO solution. (**g**) Switch-off efficiency of the sensor prepared with pristine GQDs (7.3), GQDs (18.2), or GQDs (36.2). Switch-off efficiency is noted for each size GQD.

both larger GQDs (18.2 and 36.2) effectively "turn off" HO (***Figure 3d***). However, CB[7] could not efficiently "turn on" HO (***Figure 3e***), leading to a decreased initial fluorescence (F_0) of the sensors. These two findings suggest a stronger binding affinity for HO to GQDs as its size increases, likely due to the increased surface area of larger GQDs. Upon addition of 0.25 μM of the model guest (HE) into the sensor system, HO was effectively quenched again (***Figure 3f***), resulting in a switch-off efficiency comparable to that in the small pristine GQD-based sensor. However, the dynamic range of the sensor would be inherently limited by the lower initial F_0 as size increases. Consequently, despite larger GQD-based sensors achieving a comparably high switch-off efficiency at the tested concentration of model guests, their low fluorescence intensity, dispersibility, and stability make them unsuitable for inclusion in this sensor system.

Further evaluations were also undertaken to understand the impact of GQD charge on sensor performance. The GQD surface charge was thus altered through addition of arginine surface ligands (***Figure S11a-c***).([49, 50]) In contrast to the pristine GQDs, Arg-GQDs with zeta potential of -2.0 ± 0.7 mV showed a slight reduction in the initial quenching of HO as well as a reduction in switch-off efficiency (***Figure S11d-g***), potentially attributed to the reduced negative charge of Arg-GQDs resulting in a lower binding affinity for the positively charged HO. Taken together with data for GQD size, these results point to enhanced sensor performance characteristics for use of smaller and more negatively charged GQDs. Thus, smaller pristine GQD (7.3 ± 1.2 nm) with higher charge density, exceptional dispersibility, and stability provided the optimal quencher for use in HO/GQD/CB[7] sensors and these were used in fentanyl detection for all subsequent experiments.

Detecting fentanyl and fentanyl analogues. Given an affinity of the CB[7]–fentanyl interaction of 10^7 M^{-1},([35]) comparable to the HE model guest, the HO/GQD/CB[7] sensor presented a promising approach for fentanyl detection. Their rapid, stable, and simple function could be especially effective in addressing the limitations in accessibility or reliability associated with conventional means of detection. Accordingly, this sensor was first explored for fentanyl detection by HO displacement and quenching under the same conditions as those used for the model guests. The concentration of the HO, pristine GQDs, and CB[7] were fixed at 0.25 μM, 0.5 μM, and 0.25 μM, respectively, while the fentanyl concentration was varied between 0.001–5 μM (***Figure 4a***). The sensor was prepared in DI water, with a pH of ~5.8; pH was an important parameter governing the underlying interactions explored here (*see* ***Section S.4*** *in the online supporting information*). The fluorescence emission peak at ~470 nm decreased upon increasing the concentration of fentanyl, with a complete fluorescence "off" state observed for fentanyl concentrations of 0.5 μM and above. The switch-off efficiency from these emission spectra

was then calculated, and from the resulting curve an LOD for fentanyl of 7.9 nM was derived (***Figure 4b***). By comparison, conventional immunoassay-based fentanyl test strips (FTS) using a lateral flow assay for qualitative detection of fentanyl have a practical detection limit greater than 50 nM (***Figure S12***).(22) Moreover, a recent report exploring displacement of a ferrocene catalyst from CB[7] for substrate conversion in solution could not reliably detect fentanyl below 5 mM.(46) Though the HO/GQD/CB[7] functions by a similar supramolecular displacement mechanism, use of a fluorescent reporter that is enhanced by CB[7] binding and efficiently quenched by GQDs offers significantly improved function compared to this colorimetric approach relying on catalytic conversion of a substrate in solution.

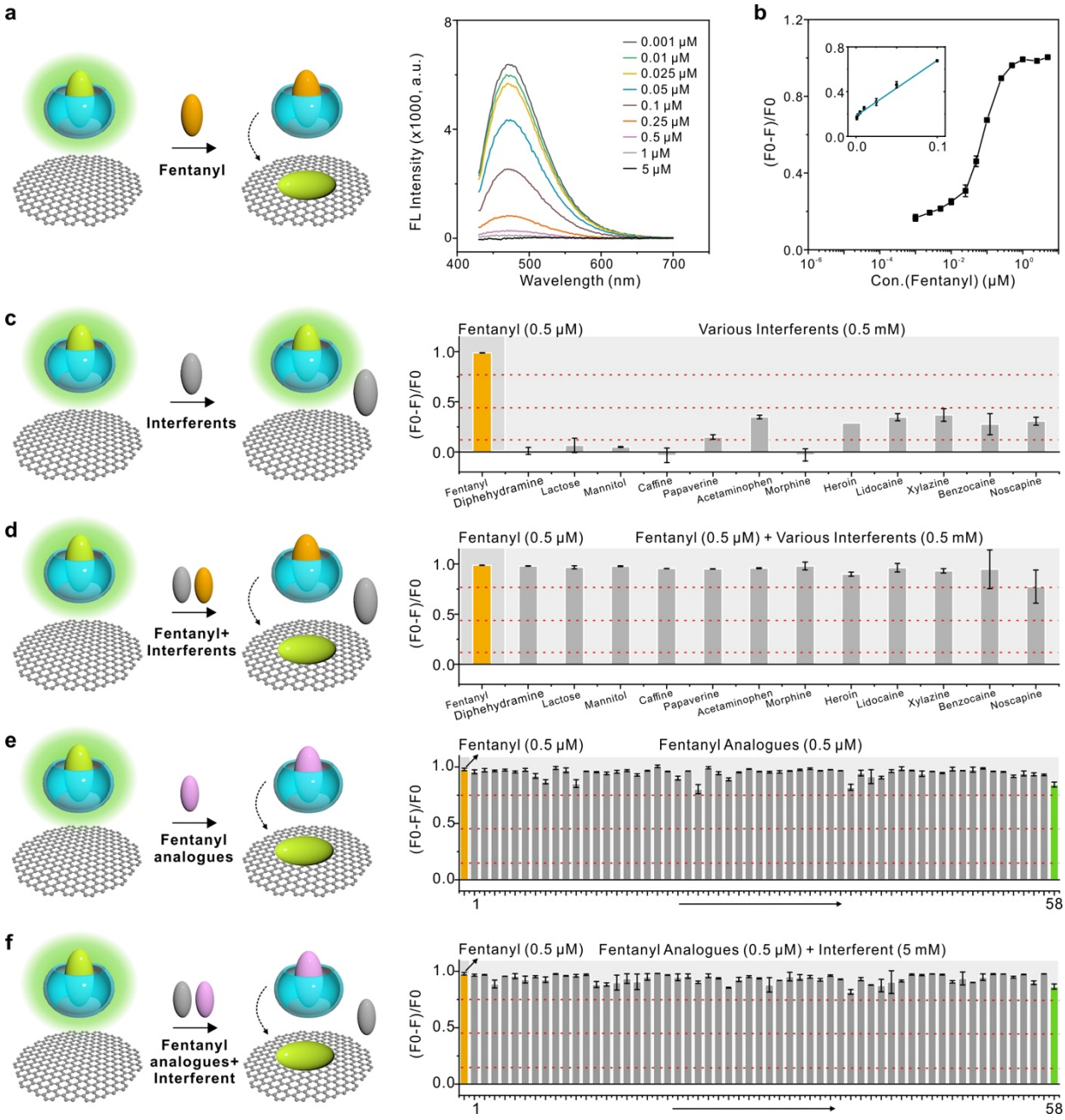

Figure 4. Sensitive and selective detection of fentanyl and fentanyl analogues using the HO/GQD/CB[7] sensor. (**a**) Fluorescence spectra of the sensor with fentanyl at increasing concentrations. (**b**) Switch-off efficiency curve and linear response (*inset*) for assays using the sensor with fentanyl at varied concentrations. A connecting line is shown only to aid in visualization of the trend. (**c**) Specificity of the sensor in detecting fentanyl (0.5 μM) compared to its signal when exposed to various common interferents (0.5 mM). (**d**) Detection of fentanyl in binary mixtures containing 0.5 μM fentanyl with 0.5 mM other interferents. (**e**) Specificity of the sensor in detecting fentanyl (0.5 μM) as well as 58 fentanyl analogues (0.5 μM). Green bar represents carfentanil. The chemical structures of the tested 58 analogues are illustrated in **Figure S16**. (**f**) Detection of fentanyl analogues in binary mixtures containing 0.5 μM fentanyl analogues with 5 mM diphenhydramine as interferent. Green bar represents mixture of carfentanil and diphenhydramine. The red dashed lines in panels **c**-**f** indicate switch-off efficiency values of 0.15 (*bottom*), 0.45 (*middle*), 0.75 (*top*). The sensor response to testing samples was assessed based on switch-off efficiency, where the criteria were defined as follows: no response if switch-off efficiency < 0.15, low response if 0.15 < switch-off efficiency < 0.45, medium response if 0.45 < switch-off efficiency < 0.75, and high/significant response if switch-off efficiency > 0.75.

Sensor selectivity was next evaluated by testing the response to interferents at a greater molar concentration (0.5 mM) relative to fentanyl (0.5 μM), aiming to simulate the composition of real-world elicit drug formulations. Interferents tested included diphenhydramine, lactose, mannitol, caffeine, papaverine, acetaminophen, morphine, heroin, lidocaine, xylazine, benzocaine, and noscapine. All of these interferent molecules produced no/low response at concentrations of 0.5 mM (***Figure 4c***, ***Figure S13***). The addition of morphine, diphenhydramine, lactose, mannitol, and caffeine to the sensor retained fluorescence identical to the blank without any interferents, yielding no response and thus had fluorescence switch-off efficiency close to 0. Accordingly, these interferents were unable to competitively displace HO from the CB[7] cavity. Samples containing papaverine, acetaminophen, heroin, lidocaine, xylazine, benzocaine, and noscapine yielded low values for switch-off efficiency (<0.45) at interferent concentrations of 0.5 mM, suggesting that these compounds weakly interact with CB[7] to displace some HO at the higher concentrations tested. Nevertheless, fentanyl (0.5 μM) induced the most pronounced response, effectively turning off sensor fluorescence and also yielding the highest switch-off efficiency of close to 1. To compare our sensor to the current standard for point-of-use detection technology, commercial FTS assays were found to yield false-positive results when diphenhydramine was at concentrations exceeding 0.5 mM (***Figure S14***). The false-positive signal from diphenhydramine and other common cutting agents is a known drawback of FTS technology.(*22*) Hence, the HO/GQD/CB[7] sensor demonstrates enhanced reliability by mitigating false-positive responses from common co-formulation agents. However, when challenged with samples containing procaine, nicotine, levamisole, MDMA, methamphetamine, quinine, and cocaine at 0.5 mM, the sensor produced false positive results with significant fluorescence switch-off response (***Figure S15***). Many of these compounds have secondary or tertiary amines adjacent to hydrophobic/aromatic groups, features that predict at least moderate CB[7] binding,(*36*) and thus likely can displace HO from CB[7] when present at the very high molar excesses studied here. Another report using CB[7] guest displacement also showed a false-positive response from methamphetamine,(*46*) which is further supported by reports for its binding affinity to CB[7] of 1.2 x 10^8 M^{-1}.(*35*) Interference from such compounds points to a drawback of CB[7]-based detection, and future work may explore use of other designer macrocycles that have demonstrated higher affinity for fentanyl.(*62*)

Given that fentanyl is often present at 1% by weight in drug samples prepared with many of the above-tested interferants,(*31*) the fluorescent sensor was next tested using binary mixtures of fentanyl and another interferent. In the binary mixtures, the fentanyl concentration was fixed at 0.5 μM, while the interferent concentration was varied from 0.5 μM to 5 mM for diphenhydramine, lactose, mannitol, caffeine, papaverine, acetaminophen. The sensor successfully detected fentanyl in all mixtures, producing a significant fluorescence response with a high switch-off efficiency close to 1 (***Figure 4d, Figure S16***). Fentanyl was also detectable in binary mixtures with varying concentrations of fentanyl (0.0025 - 0.5 μM) and fixed concentration of diphenhydramine (5 mM) as a model interferent (***Figure S17***). These findings highlighted an exceptional ability to detect low levels of fentanyl in mixtures with many interferents (up to 5 mM) containing as low as 0.01 mol% (0.5 μM) fentanyl, therefore demonstrating high sensor selectivity under relevant formulation conditions.

Toward the introduction of more potent and addictive variants, the chemistry of fentanyl has also been varied in recent years.(*63*) For instance, carfentanil is ~100 times more potent than fentanyl and is now increasingly found in seized drugs and implicated in overdose deaths. Accordingly, the HO/GQD/CB[7] sensor was explored against 58 novel synthetic fentanyl analogues and synthetic intermediates with assorted structural modifications. These variants included carfentanil, acetyl fentanyl, *meta*-methyl cyclopropyl fentanyl, *para*-methoxy acetyl fentanyl, 4'-fluorofentanyl, *para*-methyl butyryl fentanyl, hexanoyl fentanyl, 3'-methyl acetyl fentanyl, N-benzyl phenyl norfentanyl, despropionyl *para*-fluorofentanyl, *meta*-fluoro valeryl fentanyl, furanyl fentanyl, and others (*for chemical structures, see* ***Figure S18***). When tested at 0.5 μM, all of these fentanyl analogues produced a significant "turn-off" response in sensor fluorescence, yielding a high switch-off efficiency (***Figure 4e***). Excitingly, the HO/GQD/CB[7] sensor was able to detect fentanyl analogues that cannot be detected by commercial FTS, such as carfentanil, 4-Phenyl fentanyl, Despropionyl meta-Methylfentanyl, Despropionyl ortho-Fluorofentanyl, Despropionyl para-Fluorofentanyl, 4-Anilino-1-Boc-piperidine, Despropionyl 2'-fluoro ortho-Fluorofentanyl, para-fluoro 4-ANBP.(*21*, *29*, *30*) The HO/GQD/CB[7] sensor was also tested with binary mixtures of all 58 fentanyl analogues (0.5 μM) and a model interferent of diphenhydramine at 5 mM (***Figure 4f***). Again, the sensor detected all 58 analogues at 0.01 mol% in these drug mixtures. These observations demonstrated excellent detection performance with the capacity to detect at least 58 fentanyl analogues, even in drug mixtures predominated by an interferent. A prior report exploring competitive displacement from CB[7] for fentanyl detection only explored fentanyl and two analogues,(*46*) and accordingly the present work points to a much larger range of fentanyl compounds that can be detected using CB[7]-based recognition. Accordingly, this HO/GQD/CB[7] fluorescence sensor offers a highly sensitive and selective detection tool for trace amounts of fentanyl and its analogues in relevant drug mixtures.

Conclusions

Fentanyl and other opioids are responsible for the majority of drug overdose deaths in the United States. Their high potency and accessibility furthermore pose a concern for use as chemical agents. Given widespread use and exposure risk, the development of simple, rapid, reliable, and cost-effective detection tools is essential for forensics, medical care, defense, and public safety. In this work, a fluorescent sensor was developed to detect fentanyl and its analogues by using step-by-step assembly of HO, GQD, and CB[7]. The sensor

provided a fluorescence "turn-off" response enabling detection and quantification of fentanyl down to 7.9 nM. The sensor also offered robust performance in detecting fentanyl in mixtures with many common interferents, even in cases where fentanyl was at a concentration of only 0.01 mol% relative to the interferent. This is particularly relevant as fentanyl is often added to boost the potency of other agents, sometimes unbeknownst to the user.(64) The sensitivity and specificity of the sensor arises from selective host–guest complex formation between CB[7] and fentanyl, along with a low background from efficient fluorescence quenching of a the displaced reporter using GQDs. As CB[7] is able to bind to many different guests, future work is required to improve the specificity of fentanyl recognition, such as by exploring nascent macrocycles with improved binding affinity to fentanyl,(62) so as to avoid the false-positive results from agents like procaine, nicotine, levamisole, cocaine, quinine, MDMA, and methamphetamine shown here. The extensibility of this sensor to detect emergent threats was further evident in its ability to recognize 58 fentanyl analogues, even in mixtures with interferents. This sampling included detection of carfentanil, which presents an especially pressing threat given its increased availability and potency that is ~100x that of fentanyl. The sensor demonstrated rapid response time with results achieved in seconds, as well as exceptional stability over a period of 20+ days. The mode of detection should furthermore be amenable to integration within low-cost and field-ready fluorescence detection methodologies for drug testing, aligning with recent advances in the development of portable fluorescence detectors.(65) Thus, this approach could offer a first-line test to determine the presence and concentration of fentanyl in unidentified powders, seized substances, or in the context of verifying a chemical threat. However, its applicability for use in testing physiological samples (*e.g.,* blood, urine) must overcome issues related to CB[7] interactions with ambient cations,(56) while GQD may itself have issues with protein adsorption when exposed to physiological samples.(66, 67) The concentration regime for the CB[7]–fentanyl complex, with a K_d of ~55 nM,(35) also presents a challenge in interventional testing of physiological samples due to the extreme and rapid lethality of the agent at nanomolar serum concentrations. Accordingly, this sensor offers promise as a rapid, point-of-use platform for quantitative detection of fentanyl and its analogues when present at low levels or in mixtures with other many drugs, common interferents, or dispersants, contributing a tool to the arsenal of technologies aimed at improving public safety and mitigating threats from opioid exposure.

Acknowledgements

The authors gratefully acknowledge financial support from a Seed Fund of The Berthiaume Institute for Precision Health at the University of Notre Dame.

Keywords: optical sensors • drug abuse • nanotechnology • supramolecular chemistry

References:

1. P. Skolnick, The Opioid Epidemic: Crisis and Solutions. *Annu Rev Pharmacol Toxicol* **58**, 143-159 (2018).
2. Y. Zhuang, Y. Wang, B. He, X. He, X. E. Zhou, S. Guo, Q. Rao, J. Yang, J. Liu, Q. Zhou, X. Wang, M. Liu, W. Liu, X. Jiang, D. Yang, H. Jiang, J. Shen, K. Melcher, H. Chen, Y. Jiang, X. Cheng, M.-W. Wang, X. Xie, H. E. Xu, Molecular recognition of morphine and fentanyl by the human μ-opioid receptor. *Cell* **185**, 4361-4375 (2022).
3. Q. N. Vo, P. Mahinthichaichan, J. Shen, C. R. Ellis, How μ-opioid receptor recognizes fentanyl. *Nat. Commun.* **12**, 984 (2021).
4. Y. Han, W. Yan, Y. Zheng, M. Z. Khan, K. Yuan, L. Lu, The rising crisis of illicit fentanyl use, overdose, and potential therapeutic strategies. *Transl. Psychiatry* **9**, 282-290 (2019).
5. S. D. Comer, C. M. Cahill, Fentanyl: Receptor pharmacology, abuse potential, and implications for treatment. *Neurosci. Biobehav. Rev.* **106**, 49-57 (2019).
6. T. H. Stanley, The Fentanyl Story. *J. Pain* **15**, 1215-1226 (2014).
7. J. Pergolizzi, P. Magnusson, J. A. K. LeQuang, F. Breve, Illicitly Manufactured Fentanyl Entering the United States. *Cureus* **13**, e17496 (2021).
8. L. C. Smith, P. T. Bremer, C. S. Hwang, B. Zhou, B. Ellis, M. S. Hixon, K. D. Janda, Monoclonal Antibodies for Combating Synthetic Opioid Intoxication. *J. Am. Chem. Soc.* **141**, 10489-10503 (2019).
9. R. C. Barrientos, E. W. Bow, C. Whalen, O. B. Torres, A. Sulima, Z. Beck, A. E. Jacobson, K. C. Rice, G. R. Matyas, Novel Vaccine That Blunts Fentanyl Effects and Sequesters Ultrapotent Fentanyl Analogues. *Mol. Pharm.* **17**, 3447-3460 (2020).
10. J. K. O'Donnell, J. Halpin, C. L. Mattson, B. A. Goldberger, R. M. Gladden, "Deaths Involving Fentanyl, Fentanyl Analogs, and U-47700-10 States, July-December 2016" (43, US Department of Health and Human Services/Centers for Disease Control and Prevention, November 2017).
11. K. B. Palmquist, M. T. Truver, E. N. Shoff, A. J. Krotulski, M. J. Swortwood, Review of analytical methods for screening and quantification of fentanyl analogs and novel synthetic opioids in biological specimens. *J. Forensic Sci.* **68**, 1643-1661 (2023).
12. R. A. Crocombe, G. Giuntini, D. W. Schiering, L. T. M. Profeta, M. D. Hargreaves, P. E. Leary, C. D. Brown, J. W. Chmura, Field-portable detection of fentanyl and its analogs: A review. *J. Forensic Sci.* **68**, 1570-1600 (2023).
13. D. J. Angelini, T. D. Biggs, A. M. Prugh, J. A. Smith, J. A. Hanburger, B. Llano, R. Avelar, A. Ellis, B. Lusk, A. Malik Naanaa, E. Sisco, J. W. Sekowski, The use of lateral flow immunoassays for the detection of fentanyl in seized drug samples and postmortem urine. *J. Forensic Sci.* **66**, 758-765 (2020).
14. S. Buchalter, I. Marginean, J. Yohannan, I. S. Lurie, Gas chromatography with tandem cold electron ionization mass spectrometric detection and vacuum ultraviolet detection for the comprehensive analysis of fentanyl analogues. *J. Chromatogr.* **1596**, 183-193 (2019).
15. Y. Zhang, J. C. Halifax, C. Tangsombatvisit, C. Yun, S. Pang, S. Hooshfar, A. H. B. Wu, K. L. Lynch, Development and application of a High-Resolution mass spectrometry method for the detection of fentanyl analogs in urine and serum. *JMSACL* **26**, 1-6 (2022).
16. K. McCrae, S. Tobias, C. Grant, M. Lysyshyn, R. Laing, E. Wood, L. Ti, Assessing the limit of detection of Fourier-transform infrared spectroscopy and immunoassay strips for fentanyl in a real-world setting. *Drug Alcohol Rev.* **39**, 98-102 (2019).
17. X. Su, X. Liu, Y. Xie, M. Chen, H. Zhong, M. Li, Quantitative Label-Free SERS Detection of Trace Fentanyl in Biofluids with a Freestanding Hydrophobic Plasmonic Paper Biosensor. *Anal. Chem.* **95**, 3821-3829 (2023).
18. Y. Qin, S. Yin, M. Chen, W. Yao, Y. He, Surface-enhanced Raman spectroscopy for detection of fentanyl and its analogs by using Ag-Au nanoparticles. *Spectrochim. Acta A Mol. Biomol. Spectrosc.* **285**, 121923 (2023).
19. M. Zhang, J. Pan, X. Xu, G. Fu, L. Zhang, P. Sun, X. Yan, F. Liu, C. Wang, X. Liu, G. Lu, Gold-Trisoctahedra-Coated Capillary-Based SERS Platform for Microsampling and Sensitive Detection of Trace Fentanyl. *Anal Chem* **94**, 4850-4858 (2022).

20. Y. Lin, J. Sun, M. Tang, G. Zhang, L. Yu, X. Zhao, R. Ai, H. Yu, B. Shao, Y. He, Synergistic Recognition-Triggered Charge Transfer Enables Rapid Visual Colorimetric Detection of Fentanyl. *Anal. Chem.* **93**, 6544-6550 (2021).
21. J. N. Park, S. G. Sherman, V. Sigmund, A. Breaud, K. Martin, W. A. Clarke, Validation of a lateral flow chromatographic immunoassay for the detection of fentanyl in drug samples. *Drug Alcohol Depend.* **240**, 109610 (2022).
22. T.-L. E. Lockwood, A. Vervoordt, M. Lieberman, High concentrations of illicit stimulants and cutting agents cause false positives on fentanyl test strips. *Harm. Reduct. J.* **18**, 30 (2021).
23. L. Gozdzialski, M. Ramsay, A. Larnder, B. Wallace, D. K. Hore, Fentanyl detection and quantification using portable Raman spectroscopy in community drug checking. *J. Raman Spectrosc.* **52**, 1308-1316 (2021).
24. M. Smith, M. Logan, M. Bazley, J. Blanchfield, R. Stokes, A. Blanco, R. McGee, A Semi-quantitative method for the detection of fentanyl using surface-enhanced Raman scattering (SERS) with a handheld Raman instrument. *J. Forensic Sci.* **66**, 505-519 (2020).
25. C. L. O'Neal, D. J. Crouch, A. A. Fatah, Validation of twelve chemical spot tests for the detection of drugs of abuse. *Forensic Sci. Int.* **109**, 189-201 (2000).
26. C. E. Ott, A. Burns, E. Sisco, L. E. Arroyo, Targeted fentanyl screening utilizing electrochemical surface-enhanced Raman spectroscopy (EC-SERS) applied to authentic seized drug casework samples. *Forensic Chem.* **34**, 100492 (2023).
27. M. Hargreaves, *Handheld Raman, SERS, and SORS* (Portable spectroscopy and spectrometry, John Wiley & Sons, Ltd., 2021).
28. N. G. Wilson, J. Raveendran, A. Docoslis, Portable identification of fentanyl analogues in drugs using surface-enhanced Raman scattering. *Sensors Actuators B: Chem.* **330**, 129303 (2021).
29. K. L. Hayes, M. Lieberman, Assessment of two brands of fentanyl test strips with 251 synthetic opioids reveals "blind spots" in detection capabilities. *Harm. Reduct. J.* **20**, 175 (2023).
30. S. E. Rodriguez-Cruz, Evaluating the sensitivity, stability, and cross-reactivity of commercial fentanyl immunoassay test strips. *J. Forensic Sci.* **68**, 1555-1569 (2023).
31. J. Canoura, Y. Liu, J. Perry, C. Willis, Y. Xiao, Suite of Aptamer-Based Sensors for the Detection of Fentanyl and Its Analogues. *ACS Sens.* **8**, 1901-1911 (2023).
32. J. Canoura, O. Alkhamis, M. Venzke, P. T. Ly, Y. Xiao, Developing Aptamer-Based Colorimetric Opioid Tests. *Jacs Au* **4**, 1059-1072 (2024).
33. A. Shaver, N. Arroyo-Curras, The challenge of long-term stability for nucleic acid- based electrochemical sensors. *Curr. Opin. Electrochem.* **32**, 100902 (2022).
34. A. Hennig, H. Bakirci, W. M. Nau, Label-free continuous enzyme assays with macrocycle-fluorescent dye complexes. *Nat. Methods* **4**, 629-632 (2007).
35. S. Ganapati, S. D. Grabitz, S. Murkli, F. Scheffenbichler, M. I. Rudolph, P. Y. Zavalij, M. Eikermann, L. Isaacs, Molecular Containers Bind Drugs of Abuse in Vitro and Reverse the Hyperlocomotive Effect of Methamphetamine in Rats. *ChemBioChem* **18**, 1583-1588 (2017).
36. S. J. Barrow, S. Kasera, M. J. Rowland, J. del Barrio, O. A. Scherman, Cucurbituril-Based Molecular Recognition. *Chem. Rev.* **115**, 12320-12406 (2015).
37. J. W. Lee, S. Samal, N. Selvapalam, H.-J. Kim, K. Kim, Cucurbituril homologues and derivatives: new opportunities in supramolecular chemistry. *Acc. Chem. Res.* **36**, 621-630 (2003).
38. K. I. Assaf, W. M. Nau, Cucurbiturils: from synthesis to high-affinity binding and catalysis. *Chem. Soc. Rev.* **44**, 394-418 (2015).
39. C.-L. Deng, S. L. Murkli, L. D. Isaacs, Supramolecular hosts as in vivo sequestration agents for pharmaceuticals and toxins. *Chem. Soc. Rev.* **49**, 7516-7532 (2020).
40. D.-W. Lee, K. M. Park, M. Banerjee, S. H. Ha, T. Lee, K. Suh, S. Paul, H. Jung, J. Kim, N. Selvapalam, S. H. Ryu, K. Kim, Supramolecular fishing for plasma membrane proteins using an ultrastable synthetic host–guest binding pair. *Nat. Chem.* **3**, 154-159 (2010).
41. Y. C. Liu, S. Peng, L. Angelova, W. M. Nau, A. Hennig, Label-Free Fluorescent Kinase and Phosphatase Enzyme Assays with Supramolecular Host-Dye Pairs. *ChemistryOpen* **8**, 1350-1354 (2019).
42. A. T. Bockus, L. C. Smith, A. G. Grice, O. A. Ali, C. C. Young, W. Mobley, A. Leek, J. L. Roberts, B. Vinciguerra, L. Isaacs, A. R. Urbach, Cucurbit[7]uril–Tetramethylrhodamine Conjugate for Direct Sensing and Cellular Imaging. *J. Am. Chem. Soc.* **138**, 16549-16552 (2016).
43. L. Zou, A. S. Braegelman, M. J. Webber, Spatially Defined Drug Targeting by in Situ Host–Guest Chemistry in a Living Animal. *ACS Cent. Sci.* **5**, 1035-1043 (2019).
44. K. Yan, L. Wang, Z. Zhu, S. Duan, Z. Hua, P. Xu, H. Xu, C. Hu, Y. Wang, B. Di, Cucurbituril-protected dual-readout gold nanoclusters for sensitive fentanyl detection. *Analyst* **148**, 1253-1258 (2023).
45. A. S. Braegelman, R. L. Thimes, L. M. Sherman, C. J. Addonizio, S. Xian, M. Lieberman, J. P. Camden, M. J. Webber, Capture and Detection of Fentanyl with Thiolated Cucurbit[7]uril Macrocycles on Silver Nanoparticles. *ACS Appl. Nano Mater.* **7**, 10879-10885 (2024).
46. A. C. Mora, M. Vara, P. Reust, A. Code, P. Oliver, C. R. Mace, Colorimetric Detection of Fentanyl Powder on Surfaces Using a Supramolecular Displacement Assay. *ACS Sens* **9**, 3198-3204 (2024).
47. Q. Wang, L.-B. Lü, Z. Tao, T. Sun, Q. Tang, Y. Huang, The pH and mercury ion stimuli-responsive supramolecular assemblies of cucurbit[7]uril and Hoechst 33342. *Spectrochim. Acta A Mol. Biomol. Spectrosc.* **254**, 119656 (2021).
48. J. Kim, I. S. Jung, S. Y. Kim, E. Lee, J. K. Kang, S. Sakamoto, K. Yamaguchi, K. Kim, New cucurbituril homologues:: Syntheses, isolation, characterization, and X-ray crystal structures of cucurbit[n]uril (n=5, 7, and 8). *J. Am. Chem. Soc.* **122**, 540-541 (2000).
49. N. Suzuki, Y. Wang, P. Elvati, Z.-B. Qu, K. Kim, S. Jiang, E. Baumeister, J. Lee, B. Yeom, J. H. Bahng, J. Lee, A. Violi, N. A. Kotov, Chiral Graphene Quantum Dots. *ACS Nano* **10**, 1744-1755 (2016).
50. Y. Zhang, G. Kim, Y. Zhu, C. Wang, R. Zhu, X. Lu, H.-C. Chang, Y. Wang, Chiral Graphene Quantum Dots Enhanced Drug Loading into Small Extracellular Vesicles. *ACS Nano* **17**, 10191-10205 (2023).
51. G. Chakraborty, M. P. Bondarde, A. K. Ray, S. Some, Photophysical Modulation of Rhodamine-B via π-π stacking with GQD and Its Further Tuning by Cucurbit 7 uril. *Chemistryselect* **8**, (2023).
52. M. Shaikh, J. Mohanty, P. K. Singh, W. M. Nau, H. Pal, Complexation of acridine orange by cucurbit[7]uril and β-cyclodextrin:: photophysical effects and pKa shifts. *Photochem. Photobiol. Sci.* **7**, 408-414 (2008).
53. N. Barooah, A. C. Bhasikuttan, J. Mohanty, pH-Responsive supramolecular assemblies of Hoechst-33258 with cucurbiturils: Modulation in the photophysical properties. *Indian J. Chem. B* **57**, 241-253 (2018).
54. W. Lei , Q. Zhou, G. Jiang , Y. Hou, B. Zhang, X. Cheng, X. Wang, Host–Guest Interaction of Hoechst 34580 and Cucurbit[7]uril. *ChemPhysChem* **12**, 2933-2940 (2011).
55. N. Barooah, J. Mohanty, H. Pal, A. C. Bhasikuttan, Supramolecular assembly of hoechst-33258 with cucurbit 7 uril macrocycle. *Phys. Chem. Chem. Phys.* **13**, 13117-13126 (2011).
56. H. Tang, D. Fuentealba, Y. H. Ko, N. Selvapalam, K. Kim, C. Bohne, Guest Binding Dynamics with Cucurbit 7 uril in the Presence of Cations. *J. Am. Chem. Soc.* **133**, 20623-20633 (2011).
57. S. Moghaddam, C. Yang, M. Rekharsky, Y. H. Ko, K. Kim, Y. Inoue, M. K. Gilson, New Ultrahigh Affinity Host-Guest Complexes of Cucurbit[7]uril with Bicyclo[2.2.2]octane and Adamantane Guests: Thermodynamic Analysis and Evaluation of M2 Affinity Calculations. *J. Am. Chem. Soc.* **133**, 3570-3581 (2011).
58. S. M. Liu, C. Ruspic, P. Mukhopadhyay, S. Chakrabarti, P. Y. Zavalij, L. Isaacs, The cucurbit[n]uril family: Prime components for self-sorting systems. *J. Am. Chem. Soc.* **127**, 15959-15967 (2005).
59. Y. Yang, J. Liu, Z.-W. Fu, D. Qin, Galvanic Replacement-Free Deposition of Au on Ag for Core–Shell Nanocubes with Enhanced Chemical Stability and SERS Activity. *J. Am. Chem. Soc.* **136**, 8153-8156 (2014).

60. A. Ibarbia, H. J. Grande, V. Ruiz, On the Factors behind the Photocatalytic Activity of Graphene Quantum Dots for Organic Dye Degradation. *Part. Part. Syst. Char.* **37**, 2000061 (2020).
61. F. Zhang, F. Liu, C. Wang, X. Xin, J. Liu, S. Guo, J. Zhang, Effect of Lateral Size of Graphene Quantum Dots on Their Properties and Application. *ACS Appl. Mater. Interfaces* **8**, 2104-2110 (2016).
62. A. T. Brockett, W. Xue, D. King, C.-L. Deng, C. Zhai, M. Shuster, S. Rastogi, V. Briken, M. R. Roesch, L. Isaacs, Pillar 6 MaxQ: A potent supramolecular host for in vivo sequestration of methamphetamine and fentanyl. *Chem* **9**, 881-900 (2023).
63. P. Armenian, K. T. Vo, J. Barr-Walker, K. L. Lynch, Fentanyl, fentanyl analogs and novel synthetic opioids: A comprehensive review. *Neuropharmacology* **134**, 121-132 (2018).
64. S. G. Mars, D. Rosenblum, D. Ciccarone, Illicit fentanyls in the opioid street market: desired or imposed? *Addiction* **114**, 774-780 (2019).
65. Y.-H. Shin, M. Teresa Gutierrez-Wing, J.-W. Choi, Review-Recent Progress in Portable Fluorescence Sensors. *J. Electrochem. Soc.* **168**, (2021).
66. Y. Chong, C. Ge, Z. Yang, J. A. Garate, Z. Gu, J. K. Weber, J. Liu, R. Zhou, Reduced Cytotoxicity of Graphene Nanosheets Mediated by Blood-Protein Coating. *ACS Nano* **9**, 5713-5724 (2015).
67. M. Zhou, Q. Shen, J.-W. Shen, L. Jin, L. Zhang, Q. Su, Q. Hu, L. Liang, Understanding the size effect of graphene quantum dots on protein adsorption. *Colloids Surf. B* **174**, 575-581 (2019).